The Longshore Transport Enigma and Analysis of a 10-Year Record of Wind-Driven Nearshore Currents

Authors: Burnette, Carolina, and Dally, William R.

Source: Journal of Coastal Research, 34(1) : 26-41

Published By: Coastal Education and Research Foundation

URL: https://doi.org/10.2112/JCOASTRES-D-17-00010.1

Journal of Coastal Research	34	1	26–41	Coconut Creek, Florida	January 2018

The Longshore Transport Enigma and Analysis of a 10-Year Record of Wind-Driven Nearshore Currents

Carolina Burnette and William R. Dally*

Taylor Engineering Research Institute
University of North Florida
Jacksonville, FL 32224, U.S.A.

www.cerf-jcr.org

www.JCRonline.org

ABSTRACT

Burnette, C. and Dally, W.R., 2018. The longshore transport enigma and analysis of a 10-year record of wind-driven nearshore currents. *Journal of Coastal Research,* 34(1), 26–41. Coconut Creek (Florida), ISSN 0749-0208.

Previous analysis of a 10-year record of nearshore directional wave spectra collected with an Acoustic Doppler Current Profiler (ADCP) installed outside the surf zone in Melbourne Beach, Florida, unexpectedly revealed that the long-term average wave-induced radiation stress (S_{xy}) was nearly balanced between northerly and southerly forcing. More than 4 years of wind data collected at the site with a directional anemometer also showed a nearly balanced net longshore wind stress. However, shoreline offsets at nearby jettied inlets clearly indicate a predominant north-to-south net sediment transport. This enigma was investigated by analyzing the nearshore currents measured by the ADCP, and examining their correlation with the wind and incident waves. Significant correlation was found between the depth-averaged wind-driven longshore current and the incident wave conditions; *e.g.*, the average energy-based significant wave height $\bar{H}_{\mathrm{mo}}$ is typically larger (0.95 m) when the current is directed to the south than when the current is directed to the north (0.73 m). Guided by the classic Coastal Engineering Research Center (CERC) formula for longshore sediment transport, it is found that $H_{\mathrm{mo}}^{5/2}$ is significantly more correlated with southerly directed longshore currents (r = 0.47) than northerly currents (r = 0.21). Also, if a "storm" is defined as whenever H_{mo} exceeds 1.75 m, 40% of this time, the mean wave direction is out of the northeast quadrant, 33% is from the southeast, and 27% approaches shore-normal. Additionally, during storms, a stronger correlation between S_{xy} is found with southerly directed wind-driven currents (r = 0.51) than with northerly directed currents (r = 0.32). These findings indicate that net longshore sediment transport may in fact be heavily influenced by the correlation of the local wind with the waves, a feature not included in traditional longshore sediment transport formulas.

ADDITIONAL INDEX WORDS: *Nearshore waves, wind stress, ADCP measurements, longshore transport.*

INTRODUCTION

Over 10 years (28 August 2001 to 28 October 2011) of measurements of nearshore waves, currents, and water levels have been collected using an Acoustic Doppler Current Profiler (ADCP) at Spessard Holland North Beach Park in Melbourne Beach on the central Atlantic coast of Florida. This effort was originally conducted in order to monitor the long-term behavior of the wave climate in central Florida, which is expected to characterize much of the Atlantic coast of the state. The original intent was to identify any long-term trends that might help guide Florida's ongoing beach nourishment program, as well as serve as a prototype for additional permanent wave gauge installations dispersed around the state. In a thesis by Montoya (2014) and a subsequent paper by Montoya and Dally (2016), the ADCP nearshore directional wave data collected at Spessard were examined in detail. A factor of particular interest was determining if the net long-term longshore forcing induced by incident waves due to radiation stress (S_{xy}), and consequently the net longshore sediment transport, was indeed from north-to-south (N-S) as indicated by the shoreline offsets at two nearby jettied inlets. Radiation stress was computed from the fully directional spectrum (Battjes, 1972), *i.e.*:

$$S_{xy} = \int_0^{\infty}\int_{-\pi}^{\pi} E(f,\theta)\frac{c_g(f)}{c(f)}\sin(73^o-\theta)\cos\theta(73^o-\theta)d\theta\,df \quad (1)$$

in which, $E(f, \theta)$ is the frequency-direction energy density spectrum, $c_g(f)$ is the frequency-dependent group velocity, $c(f)$ is the frequency-dependent wave celerity (both computed from linear wave theory), and θ is the direction from which waves approach, positive clockwise from magnetic north. The outward normal to the local shoreline is 73° from magnetic north. With this convention, positive values of S_{xy} indicate N-S longshore forcing, whereas negative values indicate S-N longshore forcing.

Surprisingly, it was found that the net wave forcing over the 10-year period was only very slightly N-S (7.2 N/m of shoreline), whereas the standard deviation was 77.2 N/m. That is, the net was the small difference between large quantities, and, consequently, it was not as convincing an explanation as anticipated. It was also determined that it required the accumulation of 4 to 5 years of data before the net magnitude and direction of S_{xy} conclusively revealed themselves, also contrary to expectations. In addition, examination of more than 4 years of wind data (13 September 2002 to 31 December 2006) collected at the Spessard site with a directional anemometer revealed that the mean longshore component of wind stress was also essentially balanced.

In the work described herein, the current profiles measured by the same ADCP were examined in the hope that their

DOI: 10.2112/JCOASTRES-D-17-00010.1 received 16 January 2017; accepted in revision 6 April 2017; corrected proofs received 14 June 2017; published pre-print online 21 July 2017.
*Corresponding author: w.dally@unf.edu

behavior would shed light on this enigma. Offshore of the Spessard site, the bathymetry is typically smooth in the longshore direction, whereas the very nearshore profile usually contains a longshore bar. Because the ADCP was located approximately 610 m from the shoreline in 8.5 m mean depth, *i.e*. well seaward of the surf zone except during the most extreme storm events, it is justifiably assumed that the direction and intensity of the local winds supply the dominant forcing of the nearshore current, particularly near the surface. In fact, Bacopoulos *et al*. (2012) convincingly demonstrated the ability of the ADvanced CIRCulation Model (ADCIRC) (Luettich and Westerink, 2004), driven only by wind and astronomic tides, to replicate the depth-averaged longshore currents measured by the ADCP as Hurricane Jeanne made landfall in 2004, during which the largest waves in the entire ADCP record occurred (energy-based significant wave height $[H_{mo}] = 3.8$ m). Although it is well known that most of the longshore sediment flux in the nearshore takes place in the surf and swash zones, analysis of the wind-driven current outside the surf zone is relevant to modeling the shape and intensity of the longshore current inside the surf zone because the two must match at the outer limit of the surf zone. The strength of the wind-driven longshore current outside the surf zone should also be indicative of the ability of the wind to drive or enhance longshore currents inside the surf zone.

Most studies of current profiles measured with ADCPs found in the literature have been conducted well off the coast (15–30 km) and at greater depths (12–25 m) than was the case at the Spessard site, *e.g*., Book *et al*. (2007), Cosoli, Gacic, and Mazzoldi (2008), Münchow and Chant (2000), and Whitney and Garvine (2005). In addition to direct wind stress, in these studies, buoyancy, baroclinic, Coriolis, and frictional effects were found to be factors in determining the strength, vertical structure, and spatial patterns of the mean flows. To the contrary, it is generally assumed that currents in the surf zone are mainly wave-driven features, and that the tail of the longshore current outside the surf zone and in the nearshore is induced by lateral mixing of the wave-driven surf zone current (Longuet-Higgins, 1970; Svendsen and Putrevu, 1994). With few exceptions, it is consequently assumed in engineering practice that longshore sediment transport in the surf zone and nearshore is solely a wave-driven phenomenon (*e.g*., USACE, 2002). However, early studies, such as that by Murray (1975) using drogues, and that by Nummedal and Finley (1978), based on visual estimates of littoral conditions, found that the wind played the major role in driving nearshore and surf zone currents. Using electromagnetic current meters and dye deployments, Hubertz (1986) collected measurements of nearshore and surf zone currents on several occasions between 1982 and 1984 at the USACE Field Research Facility in Duck, North Carolina, and his results also showed the importance of winds in driving these currents.

At this point, it is noted that in a wave and beach processes modeling study from Sabine Pass to Galveston Bay, Texas, King (2007) encountered the issue that, although it is well established that the net longshore transport along this coast is from NE to SW, initial attempts using the Generalized model for Simulating Shoreline change [GENESIS] (Gravens, Kraus, and Hanson, 1991; Hanson and Kraus, 1989) driven by Wave Information Study (WIS) hindcast wave information (1990–99) produced net transport in the opposite direction. Based on the observations of the importance of local winds on longshore currents noted by several researchers that had worked in the region in the past, King (2007) introduced wind forcing into the Coastal Engineering Research Center (CERC) formula (USACE, 2002) and was subsequently able to correct the direction of net transport.

In regard to cross-shore surface currents outside the surf zone, although the strength is mostly determined by the cross-shore component of wind shear, the wave-induced Stokes drift, and any tide-induced flow (Murray, 1975), it is the requirement for balance in the depth-integrated cross-shore mass flux imposed by the proximity of the shoreline that exerts the greatest influence on the profile shape of the cross-shore currents below the mean water level, with additional influence exerted by the presence or absence of temperature stratification (Murray, 1975). However, this return-flow condition is of course not imposed on the longshore current, and it is the strength of the longshore component of the nearshore current and its correlation with local wind and waves that will be the main focus here in the search for an answer to the longshore transport enigma.

Perhaps most importantly, the nearshore current studies presently found in the literature are generally based on short-term records, typically on the order of a few weeks to a year. As will be shown herein, the availability of measurements collected for a decade from the Spessard station allows seasonal and longer-term analyses of longshore and cross-shore currents in the nearshore to be conducted, and consequently their roles in various littoral processes at large temporal scales to be postulated. Examination of the behavior of currents outside the surf zone and evaluation of their correlation with the wind not only help to delineate their role in nearshore sediment transport, this type of analysis can shed light on the likely importance of currents outside the surf zone in larval transport and the behavior of oil spills and pathogen outbreaks in the nearshore.

METHODS

The data collection station utilized in this study was located at Spessard Holland North Beach Park in Melbourne Beach, on the open coast of east-central Florida between Port Canaveral, 38 km to the north, and Sebastian Inlet, 24 km to the south, as shown in Figure 1. Both of these entrances are jettied, with shoreline offsets that indicate net N-S longshore transport (see Figure 1 of Montoya and Dally, 2016).

Instrumentation and Data Collection

The ADCP used was the RD Instruments Sentinel 1200 kHz model, which was attached to the top of a jetted pipe (spud) so that the instrument was elevated sufficiently above the bed to avoid burial by sediment. As opposed to a bottom-resting frame, the spud always maintained its vertical orientation and did not scour or settle into the bed. Two different spud locations, approximately 55 m apart, were used during the data collection. Spud #1 was located at 28°3.370′ N; 80°32.672′ W, with a gauge altitude of approximately 1 m above the bed, whereas spud #2 was located at 28°3.355′ N; 80°32.701′ W, with

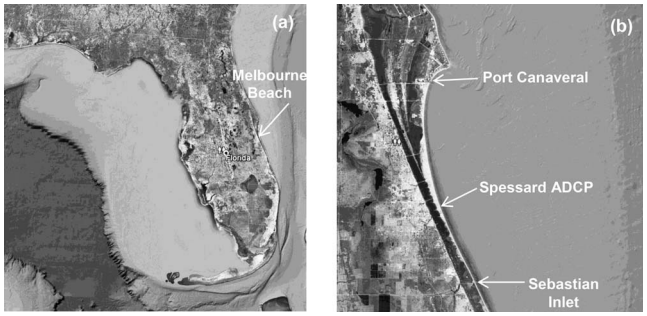

Figure 1. (a) Florida Peninsula showing the location of Melbourne Beach. (b) The locations of Port Canaveral (Trident Pier tide gauge), the Spessard ADCP, and Sebastian Inlet.

a gauge altitude of 1.6 m above the bed. The instrument was cabled to a shore station, which provided power and communication, enabling data to be reported directly to a website via cell phone. Whenever a cable or instrument malfunction occurred, a self-recording ADCP was installed on the spud as soon as possible. Additional details of the operation of the station are available in Montoya and Dally (2016).

The sampling scheme for current profiles varied during the first few years of operation, but the majority of the profiles were constructed by averaging 200 pings over 10 minutes (*i.e.* a sampling rate of 0.33 Hz). ADCP operations were conducted from 28 August 2001 until 28 October 2011, with a 95% data capture rate. For reference, wave data were sampled at 2 Hz in 20-minute bursts every 2 hours over the same time period.

The ADCP was equipped with a pressure transducer for estimating the elevation of the mean water level above the instrument, neglecting barometric correction. However, the transducer proved to be prone to clogging during long deployments and experienced malfunctions several times, which rendered the measurements of mean water depth unreliable for extended periods. As a consistently collected substitute, the 6-minute water elevation record from the National Oceanic and Atmospheric Administration (NOAA) tide gauge station #8721604 at the Trident Pier, located 30 km to the north at Port Canaveral (see Figure 1), was used to supply the mean water depth over the entire 10-year period of data collection at Spessard. Based upon careful correlation with the reliable segments of the depth record from the ADCP, the NOAA time series was shifted 12 minutes to compensate for the tidal phase lag between the Spessard and Trident Pier locations.

The weather station at Spessard included an R.M. Young directional anemometer mounted to a 10 m tall tower, installed at the top of the local dune. Although containing some gaps in the record, the instrument operated from 13 September 2002 until 20 June 2005, when it was destroyed by a lightning strike. It was subsequently replaced with a new instrument on 6 October 2005, which operated reliably until 31 December 2006. In the analysis here, wind data from an anemometer installed at the Trident Pier (also an R.M. Young model) were used for the years 2002 and 2007–11, as well as to fill in the gaps in the Spessard record. Comparison of the Trident wind data to the Spessard measurements during the overlapping time period of 2003–06 generally showed close agreement.

Current Profile Processing

The raw data files from the ADCP were processed using the manufacturer's proprietary software called WavesMon, which, in addition to current profiles, computes directional spectra and wave parameters. The processing software generates speed and direction for the bins above the blanking distance of the instrument. Initially, the ADCP was programed to collect current data from 26 bins, each 0.30 m in height, with a blanking distance of 0.83 m. Later in 2005, it was changed to 16 bins, each 0.50 m in height, with a blanking distance of 1.05 m. As described below, the number of bins, their respective width, and the blanking distance were taken into account in assembling the currents files for each year in a consistent manner.

Figure 2 presents a sample of the distribution of currents from 23 February to 1 March 2002, displaying the elevation above the blanking distance of the instrument on the left scale and the bin number on the right. It is clear that the ADCP often "measured" above the mean water surface, and these are considered to be false returns. Book *et al.* (2007) investigated the contamination of their ADCP measurements at the surface of the water in detail and suggested truncating the current profile at a distance of 6% of the total water depth. The present study examined the structure and intensity of the currents throughout the majority of the water column, with particular interest in the correlation between local winds and the behavior of the upper layers. Consequently, in order to have

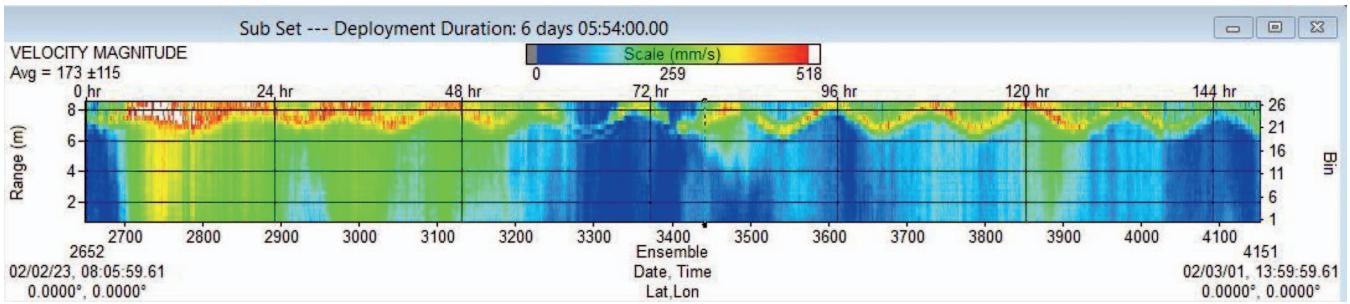

Figure 2. Example distribution of currents from 23 February to 1 March 2002, showing fictitious returns from above the mean water level.

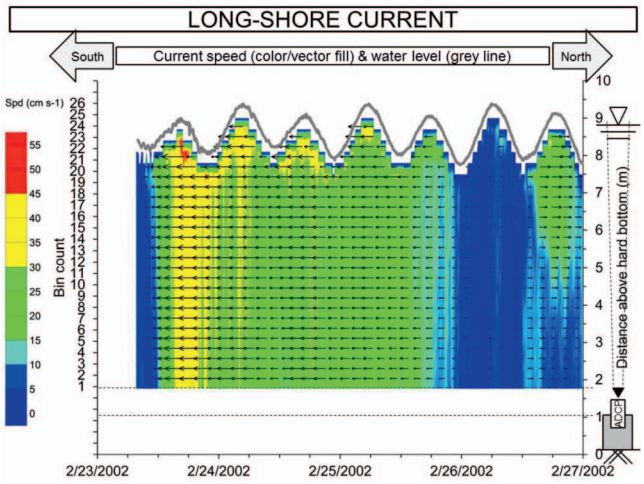

Figure 3. Example time series of the vertical distribution of the longshore current (V) after redacting measurements within 6% of the distance to the mean water level (23–27 February 2002).

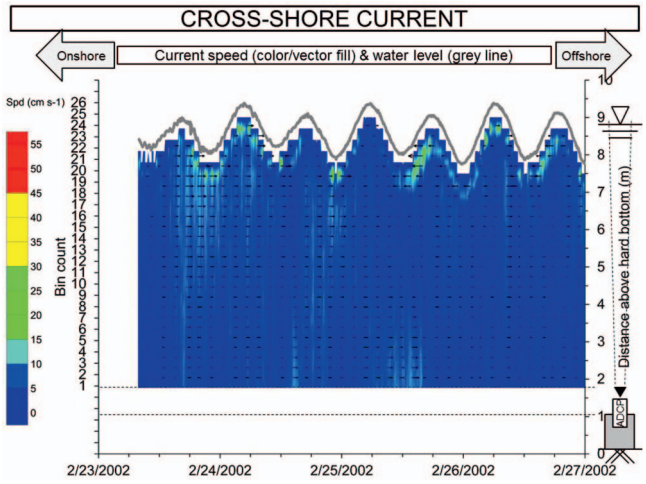

Figure 4. Example time series of the vertical distribution of the cross-shore current (U) after redacting measurements within 6% of the distance to the mean water level (23–27 February 2002).

as reliable a near-surface record as possible, the entire 10 years of current data were screened by truncating the top of the current profile at the elevation representing 6% of the total water depth below the (tide gauge–defined, 6-minute average) water surface. In other words, edited current data extend to the mean sea-surface elevation minus 6% of the total water depth above the instrument, as recommended by Book *et al*. (2007).

The currents measured by the ADCP were directed "to-which" relative to magnetic north, whereas the winds originally used the convention "from-which" relative to magnetic north. The wind record was rotated to the "to-which" convention, and with the shoreline oriented nominally 17° west of magnetic north, a direction of 253° from magnetic north is regarded as flowing normal to the shoreline in the onshore direction for both wind and currents. The record of currents was decomposed into the cross-shore component (U) being positive going nominally from W to E (253° towards 73°), and the longshore component (V) being positive going from nominally S to N (163° towards 342°). It is noted that this sign convention is opposite to that adopted by Montoya and Dally (2016) for S_{xy} (positive was N to S). Samples of the time series from 23 February 2002 (0800 hours) until 27 February 2002 (0000 hours) of the vertical distribution of longshore and cross-shore currents, after redacting the data just below the mean water level as described above, are provided in Figures 3 and 4, respectively.

Normalizing Elevations above the Instrument and Temporal Averaging

The processed current data provide speed and direction for every one of the equally distributed bins above the instrument blanking distance, through the water column. In conducting the analysis, to meaningfully examine the response of the currents to wind forcing, it is necessary to render the physical elevation of the acoustic bins in the water column to normalized elevations, in order to compensate for the fluctuating tide. Normalization was accomplished simply by dividing the physical bin elevation by the total mean water depth during each current burst. After normalizing, the data were vertically interpolated into a matrix with 21 rows going from 0 to 1 on a nondimensional scale. For initial analysis, each time series (row) was then subjected to 2-hour block averaging, which reduced the number of points in the time series from nominally 52,560 points per year to 4380. As an example, for the year 2004, Figures 5 and 6 present time series of the upper layer of the normalized water column with the velocity vectors averaged every 2 hours as noted above. The cross-shore component of the current is positive pointing to the right (offshore), and the longshore component is positive pointing up.

RESULTS

After processing and conditioning the data, the longshore and cross-shore current profiles were each subjected to (1) averaging and basic statistical analyses by year, (2) monthly averaging, and (3) depth integration to estimate volume fluxes for both longshore and cross-shore directions. Correlations of the currents with both the wind and the incident waves were then examined.

Annually Averaged Profiles and Annually Based Statistics

Yearly averages of the vertical profiles of the longshore current produced only a small residual of many large positive (north) and large negative (south) values, as was found by Montoya and Dally (2016) for S_{xy} (noting the difference in sign convention). Nevertheless, Figure 7 presents the annual mean profiles of longshore current for each year in the record. The net longshore surface current each year is somewhat surprisingly directed towards the north, although it varies greatly in magnitude from year to year. However, below an elevation generally found at approximately 0.4 normalized elevation, there is indication of a reversal, with mild southerly flow.

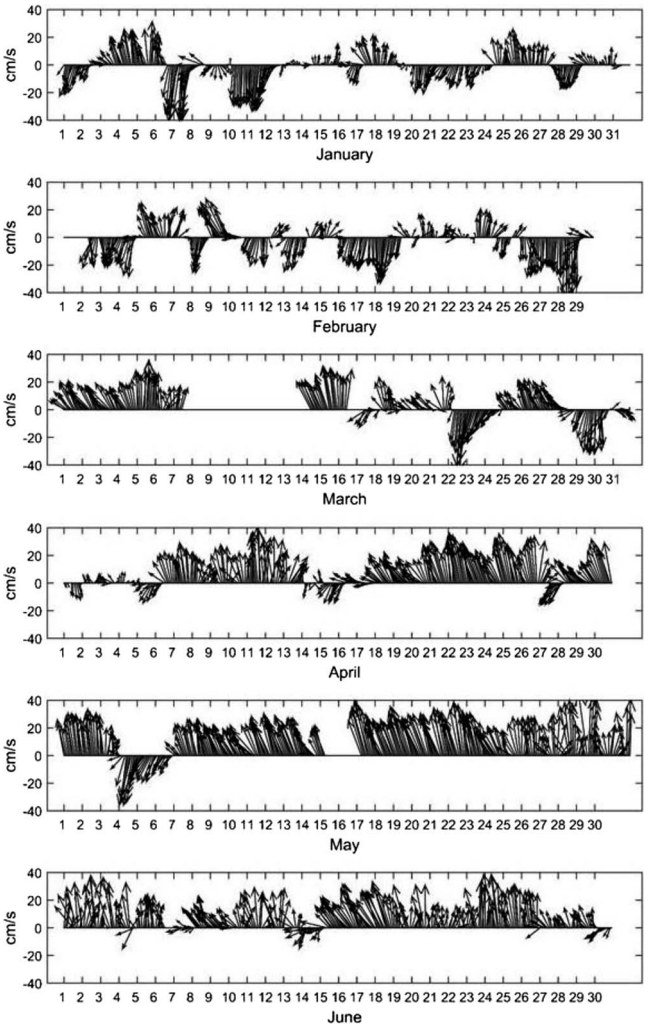

Figure 5. Example time series of the 2-hour block-averaged current vectors for the upper layer of the depth-normalized water column (0.95) from January to June 2004.

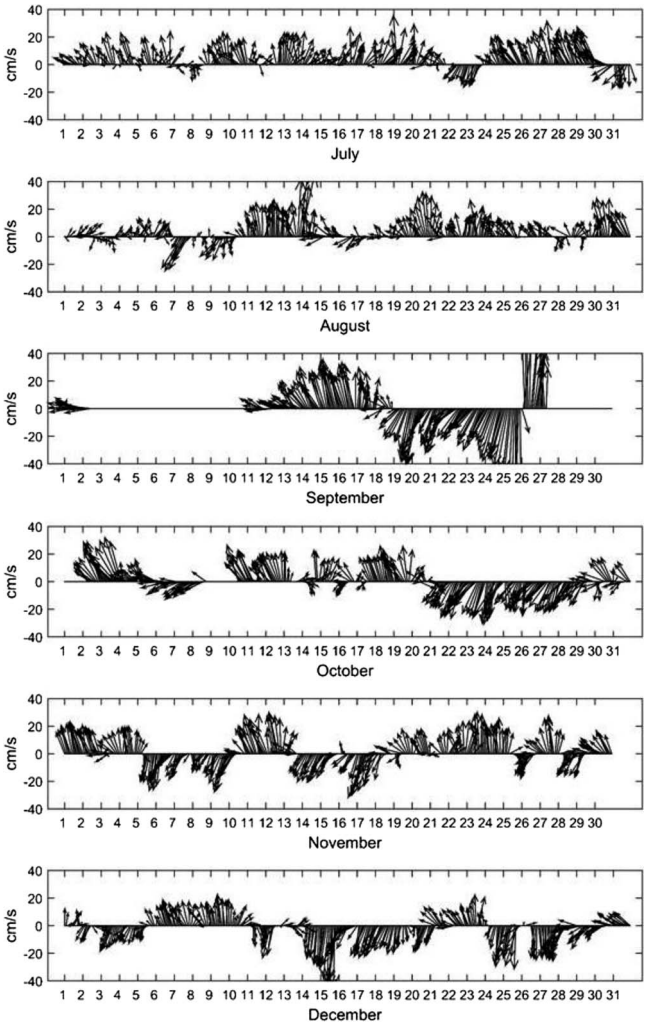

Figure 6. Example time series of the 2-hour block-averaged current vectors for the upper layer of the depth-normalized water column (0.95) from July to December 2004.

Unfortunately, the elevation of the instrument above the bed and its blanking distance precluded measurements in the lowest portion of the water column. The mean profile of the annualized longshore current shows larger magnitudes in the upper layers of the water column than at the bottom for all years except 2003 and 2007, and yet the shape of the profiles is notably self-similar for all years. (Although data collection stopped on 28 October, 2011 was regarded as a "complete" year.)

Contrary to the large variation in the magnitude of the annually averaged longshore current profiles presented in Figure 7, the annually averaged cross-shore current profiles presented in Figure 8 are tightly grouped, with strong onshore flow in the upper water column, one zero-crossing point around 0.90 normalized elevation, and milder offshore return flow that recurves and typically diminishes rapidly with depth. This indicates a lack of vertical mixing in the cross-shore direction as compared to the longshore direction, with cross-shore stagnation in roughly the lower half of the water column. This structure could be induced by temperature stratification (Houghton and Woods, 1969; Murray, 1975), particularly during heating of the surface layer during summer months, as well as during upwelling events.

The 10-year current record was also subjected to an annual statistical analysis. First, five evenly spaced levels in the normalized water column were selected, with the bottommost level at 0.35 normalized elevation and the uppermost at 0.95. This approach reduced the number of levels examined from 20 to 5, facilitating the interpretation of the results while keeping enough information to convey the vertical structure and variability of the currents. Basic statistical properties, *i.e.* the mean, standard deviation, and maxima, were determined annually for the longshore current and the cross-shore current in each of the five layers, with the results provided in Table A1

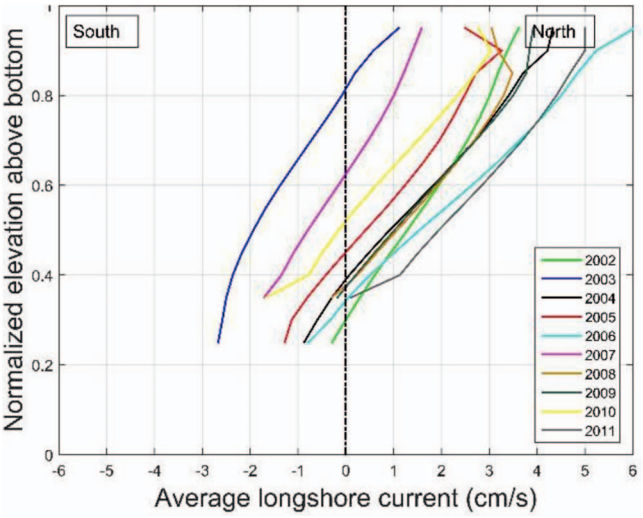

Figure 7. Annual mean depth-normalized profiles of the longshore current.

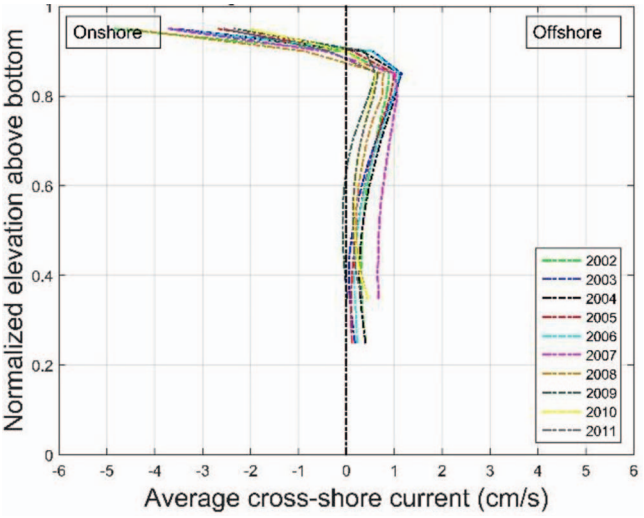

Figure 8. Annual mean depth-normalized profiles of the cross-shore current.

in Appendix A. At all five elevations, the standard deviation of the longshore current is an order of magnitude greater than the mean (Figure 7), and it consistently decreases in amplitude from the surface to the bottom. The strongest northerly value was 124.7 cm/s, and the strongest southerly value was –97.8 cm/s, both associated with the landfall of Hurricane Jeanne (26 September 2004), and both found at 0.95 normalized elevation. For the cross-shore current, the annual mean was consistently and strongly onshore at the 0.95 elevation, and weakly offshore below, as seen in Figure 8. The standard deviation is again generally an order of magnitude greater than the mean, and it is greatest in the uppermost layer. However, the annual standard deviation in the cross-shore current is consistently uniform in the four lower layers. The year 2009 experienced the strongest offshore current of 130.9 cm/s, and 2008 had the strongest onshore current of –103.9 cm/s, with both occurring at 0.8 normalized elevation.

Monthly Averaged Longshore Current Profiles

Averaging the vertical profiles of the longshore current by month showed that the surface currents are usually toward the south during the winter and toward the north in the summer; however, in spring and fall, they are mixed. This seasonality is demonstrated in Figure 9, which presents the mean profiles for the months of March, June, September, and November for each of the 10 years of measurements. The mean longshore currents in November are almost uniform with depth, whereas those in June display distinct vertical structure. Currents in March and September possess only slight vertical structure.

Volume Flux

Unfortunately, there were no velocity measurements close to the bottom due to the elevation of the instrument above the bed and its associated blanking distance, as well as above the near-surface cutoff elevation. Nevertheless, examination of the total volume flux in the measureable water column yields useful results. Returning to the original time series of 10-minute-averaged current profiles, summing the mean longshore and cross-shore currents over the bins of the dimensional water column produces the volume flux for each component:

$$Q_L = \sum_{i=1}^{N} V(z)\Delta z; Q_C = \sum_{i=1}^{N} U(z)\Delta z \qquad (2)$$

where, Q_L is the volume flux ($m^3/s/m$) in the longshore direction, Q_C is the volume flux ($m^3/s/m$) in the cross-shore direction, N is the number of physical bins measured in the water column during a particular 10-minute sample, and Δz is the physical width of each bin. Figure 10 presents a day-long running average of the volume flux for 2003, where it is evident that Q_L is predominantly towards the south. Q_C is an order of magnitude less, and the net is directed offshore. If measurements were available both above the uppermost bin, where wave-induced Stokes drift takes place (Starr, 1947), and between the blanking elevation and the bottom, ideally the total cross-shore volume flux would always be zero, unless there is large-scale circulation present (*e.g.*, gyres or rip currents). Figure 11 presents a similar plot for 2004, where Q_L is predominantly toward the north. The net Q_C is again offshore; however, as noted, this is problematic because of the lack of data in the extreme upper and lower parts of the water column.

Table 1 presents the annually averaged volume flux results for each one of the 10 years in the record, as well as the mean and standard deviation for all values. As was indicated in Figure 7, the mean vertical profile of the longshore current for most of the years was oriented toward the north, although 2003 and 2007 were southerly directed. The average net longshore volume flux above the lowest bin for the entire 10 years is 0.08 $m^3/s/m$, with a standard deviation of 0.07 $m^3/s/m$. Although the net is towards the north, an estimate of the apparently southerly volume flux near the bed is unobtainable. The total cross-shore annually averaged cross-shore

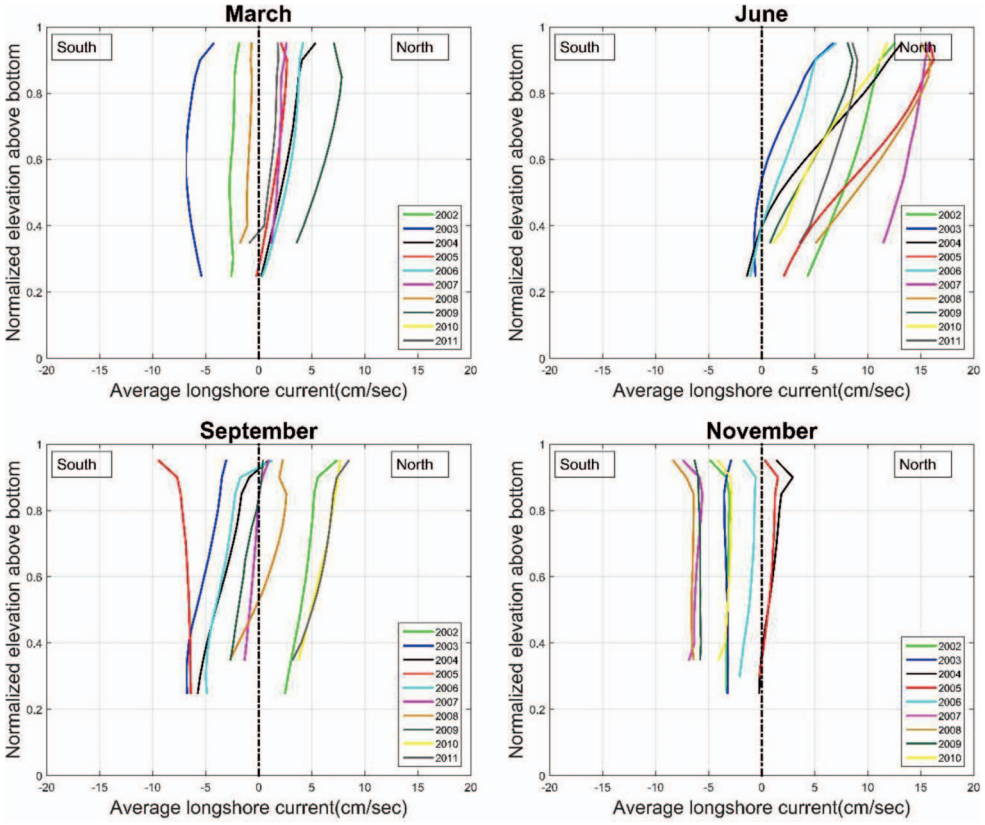

Figure 9. Depth-normalized mean profiles of the longshore current for the months of March, June, September, and November for each year of the record.

volume fluxes for each year, and the average over the 10 years of 0.003 $m^3/s/m$ are more than an order of magnitude smaller than the longshore results, indicating an almost balanced cross-shore flux, as anticipated given the proximity of the shore boundary.

Correlation of Currents with the Wind

As mentioned in the introduction, Hubertz (1986), Nummedal and Finley (1978), and others have found that local winds play an important role in driving the longshore current in the nearshore and surf zone. In the present study, in order to analyze the entire record of available current profiles, 4 years of wind measurements from the Spessard station (2003–06) and nominally 6 years of wind measurements from the Trident Pier NOAA station (2002, 2007–11) were utilized. Correlations of wind vectors with the currents at the surface, middepth, and at the blanking elevation of the ADCP were first qualitatively examined. Then, the correlations between the longshore wind speed and the vertically averaged longshore currents, and between the cross-shore wind speed and vertically averaged cross-shore currents were quantified on a monthly basis over a composite ensemble of the 10 years of observations. Computed wind stress was also examined, and the strong seasonal correlation between its longshore component and the vertically averaged longshore current was demonstrated.

Wind Speed and Direction

Current velocity vectors, again employing 2-hour block-averaging, were constructed for the upper layer (0.95), the middle layer (0.65), and the bottom layer (0.35) from the depth-normalized longshore and cross-shore profiles and were examined together with 2-hour average wind velocity vectors. Figure 12 presents a summer month (June 2003) during which the winds were predominantly directed toward the north. The wind speed and direction (upper panel) and the current speed and direction in the upper layer of the water column (second panel) are obviously highly correlated. However, in the lower layer, the wind did not force the current with the same intensity, as should be expected. In summer, winds typically blow S-N, and their magnitudes are smaller than the N-S winter winds. Consequently, during weak wind conditions, it is common to find current reversals between the upper and the lower layers of the water column as, *e.g.*, from 14 to 18 June.

Figure 13 presents data for a winter month (November 2003), where the strong correlation between the wind speed and direction (upper panel) and the current speed and direction in the upper layer of the water column (second panel) is clearly evident. Also, when the winds are directed nearly alongshore, the currents move in the same direction through the entire water column, as is seen for 8–11 November, 18–19 November, and 29–30 November. Otherwise, when winds have a strong onshore component (to the left), the upper layer of the current

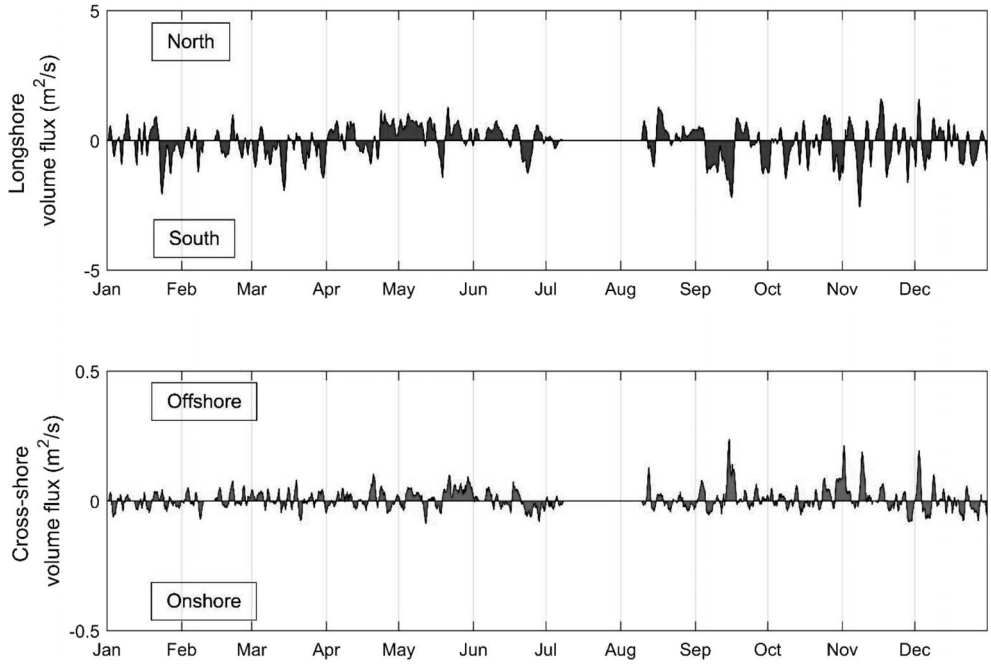

Figure 10. Daily running average of longshore volume flux and cross-shore volume flux for 2003, indicating that the net longshore volume flux is towards the south, and the net cross-shore volume flux is an order of magnitude less.

profile follows suit, whereas the middle and lower layers display compensating offshore flow.

The upper panel of Figure 14 presents, on a monthly basis, a composite over the 10 years of the correlation between the time series of the 2-hour-average longshore wind speed and the 2-hour-average longshore current, in both the upper and lower layers of the water column. The bottom panel of the figure presents the results for the cross-shore wind speed and cross-shore current. The composite year clearly shows seasonal patterns: The longshore current in the upper layer is highly correlated with the longshore component of the wind speed for the winter months, but there is markedly reduced correlation in the summer months. The correlation of the lower layer of the longshore current is always less than the upper layer, but it consistently follows the same pattern. In the lower panel, the cross-shore current in the upper layer of the water column is moderately correlated with the cross-shore component of the wind speed for most months, but, interestingly, for most of the winter months, the correlation is slightly less than in the spring and summer months. In the lower layer, the correlation is negative due to the offshore-directed return flow during onshore winds, but with lower magnitudes in the summer than in the other seasons.

Wind Stress

The wind stress vector, $\bar{\tau}$, for each 10-minute average provided by the Spessard and Trident Pier anemometers can be estimated using:

$$\bar{\tau} = \rho_a C_d \vec{W}_{10} |\vec{W}_{10}| \quad (3)$$

in which, ρ_a is air density ($\sim$1.2 kg/m^3), $\vec{W}_{10}$ is the wind velocity (m/s) at 10 m elevation above the ground, and C_d is a drag coefficient calculated as proposed by Garrett (1977):

$$C_d = 0.001(0.8 + 0.065|\vec{W}_{10}|) \quad (4)$$

Decomposition of the wind stress into longshore and cross-shore components was performed, from which yearly averages were computed. Table 2 shows that during the entire record, although 4 out of the 10 years had a positive (S-N) average longshore wind stress, the mean for the 10 years is –0.0003 N/m^2, with a standard deviation of 0.0013 N/m^2. This confirms that there is only a slight N-S bias in the wind stress for the 10-year record, consistent with the findings of Montoya and Dally (2016). For the cross-shore wind stress, Table 2 also shows that 8 of the 10 years had negative (onshore) wind stress. Furthermore, the mean is –0.0056 N/m^2, with a standard deviation of 0.0060 N/m^2; *i.e.* the mean onshore stress is an order of magnitude greater than the mean longshore stress for the 10-year record.

In order to examine the mean seasonal behavior and correlation of the longshore currents with the longshore component of the wind stress, a 2-hour block-averaged time series of the depth-averaged current was constructed for each one of the 10 years of record. Again, it is noted, however, that the depth averaging was not over the entire water column due to the height of the instrument above the bed and the acoustic blanking distance (Figures 7 and 9). Also, because of the various gaps in the ADCP record, these 10 time series were then used to create a composite year of longshore current by averaging the available data at each 2-hour time block. Figure 15 presents a weekly running average for the longshore current

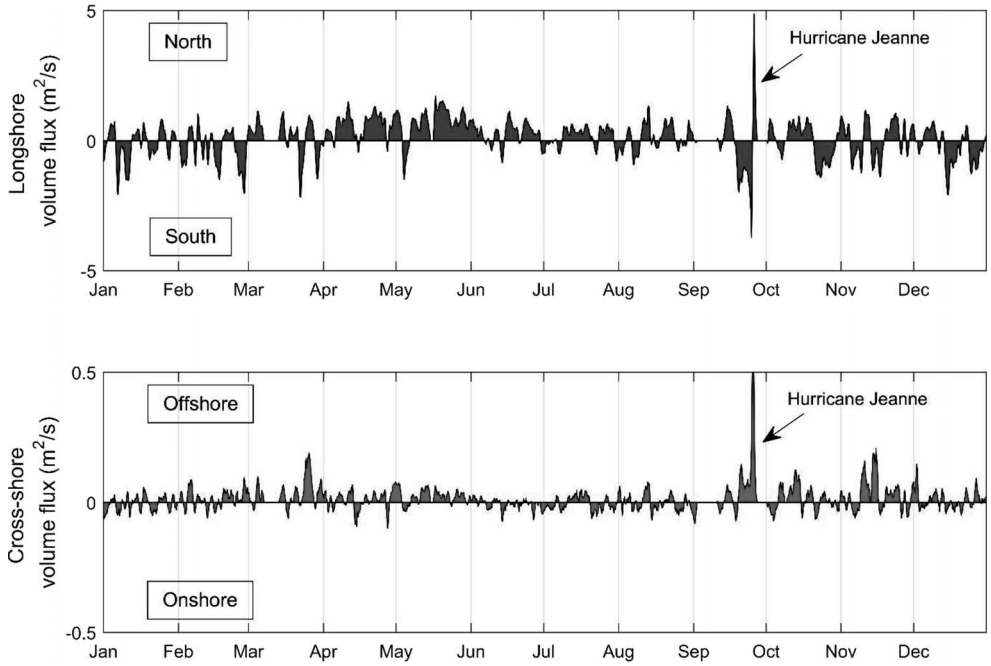

Figure 11. Daily running average of longshore volume flux and cross-shore volume flux for 2004. The net longshore volume flux is directed toward the north, and the net cross-shore volume flux is offshore.

for the composite year (upper panel). The seasonality of the current is clearly evident, with a dominant longshore current directed to the north during the summer months, and a dominant current directed toward the south during the winter months. Similarly, a composite year was constructed from the 2-hour averaged time series of the computed longshore wind stress, and a weekly running average for the composite year is presented in the lower panel of Figure 15. Again, the seasonality is clearly evident, with a dominant northerly directed stress during the summer months, and a prevailing southerly stress during the winter months. Although the net longshore wind stress is slightly to the south (Table 2), it appears in the upper panel as though the net discharge would be towards the north. However, this is inconclusive, because the entire water column was not measured. As is visually apparent, however, in Figure 15, the two composites are highly correlated, with $r = 0.91$.

DISCUSSION

Based on (1) the findings of Montoya and Dally (2016) for the near-balance in wave-induced radiation stress, (2) the apparent northerly bias in the composite depth-averaged longshore current measured by the ADCP (Figure 15, upper panel), and (3) the wind analysis for the longshore direction conducted thus far (Figure 15, lower panel), the reason for the distinct long-term net N-S sand transport along the central Brevard County coast has not convincingly revealed itself. However, if the correlation between the longshore component of the nearshore currents and the local waves measured with the ADCP is examined, particularly during storms, the likely solution to the enigma becomes apparent.

Correlation of Longshore Currents with Radiation Stress and Wave Height

Although the currents measured at the ADCP are presumed to be predominantly wind-driven features, one might expect some correlation between the currents and the radiation stress associated with the incoming waves, *i.e.* negative correlation with S_{xy} as defined by Equation (1). Perhaps surprisingly, if the entire record is utilized, the radiation stress and the vertically averaged longshore current at the ADCP are found to be essentially uncorrelated, with the magnitude of annually computed coefficients typically less than 0.1. However, examining the correlation of the longshore currents with the waves simply by averaging the significant wave height (H_{mo}) reported by the ADCP when the depth-averaged current is to the south, separately from the times when it is to the north, is quite revealing. Table 3 presents the results, and it is seen that, without exception, for each of the 10 years, the average H_{mo} is smaller when the (wind-driven) longshore current is heading to the north than when the current is going to the south, with their averages being 0.73 m and 0.95 m, respectively. If the direction and intensity of the wind-driven nearshore current at the ADCP are indicative of characteristics inside the surf zone, then surf zone processes governed by wave height, or powers thereof, would be expected to exhibit a distinct N-S bias as well. This is pursued further next.

Longshore Transport Inferred from Correlation with $H_{\mathrm{mo}}^{5/2}$

The commonly used CERC formula for longshore sand transport (USACE, 2002), *i.e.*:

Table 1. *Annually averaged longshore ($\bar{Q}_L$) and cross-shore ($\bar{Q}_C$) volume fluxes.*

Year	$\bar{Q}_L$ (m^3/s/m)	$\bar{Q}_C$ (m^3/s/m)
2002	0.11	0.0002
2003	−0.08	0.0007
2004	0.10	0.0130
2005	0.05	0.0100
2006	0.15	0.0080
2007	−0.01	0.0110
2008	0.10	−0.0090
2009	0.11	−0.0060
2010	0.05	0.0010
2011	0.17	−0.0030
Mean	*0.08*	*0.0030*
Stand. Dev.	*0.07*	*0.0070*

$$Q_{ls} = 0.46\rho_w g^{3/2} H_{bs}^{5/2} \sin\alpha_b \cos\alpha_b \quad (5)$$

in which, Q_{ls} is the total longshore transport in m^3/d, ρ_w is the mass density of seawater, g is gravity, H_{bs} is the significant wave height at incipient breaking, and α_b is the wave angle relative to the bottom contours at incipient breaking, prescribes a 5/2 power on significant wave height based upon the hypothesis that gross transport is proportional to the "longshore component of wave energy flux per unit length of beach" (*cf.* Komar, 1979). Utilizing the entire record of currents and waves, Table 4 presents the correlation of longshore currents with $H_{mo}^{5/2}$ at the ADCP, and it is seen that a much stronger correlation (r = 0.47) exists between southerly directed currents and $H_{mo}^{5/2}$ as compared to the correlation with northerly directed currents (r = 0.21). Although the radiation stress and the longshore wind stress at the Spessard site would appear to be nearly balanced separately, as found by Montoya and Dally (2016), this correlation of $H_{mo}^{5/2}$ with the wind-induced current outside the surf zone points to a plausible explanation for the net long-term N-S transport known to characterize the region. That is, a similar correlation should be expected with the wind-enhanced current/transport inside the surf zone.

Annual Storm Analysis

Hypothesizing that, although occurring intermittently, storms dominate the net longshore transport climate, and following Montoya and Dally (2016), an individual storm is somewhat arbitrarily defined herein as whenever H_{mo} exceeds 1.75 m in a points-over-threshold sense with a 72-hour window. That is, all wave height data that exceed 1.75 m within a 72-hour period are collectively identified as a single storm. Nominally, 6% of the data exceeded this 1.75 m threshold. The storm count for each calendar year is presented in Table 5, showing that 2004, 2005, 2006, 2008, and 2011 were very active, with a total of 11–12 storms each year. (Note: The H_{mo} "data" from 28 October to 31 December 2011 were extracted from a nearshore synthetic wave record developed as described in Dally and Osiecki [2006].)

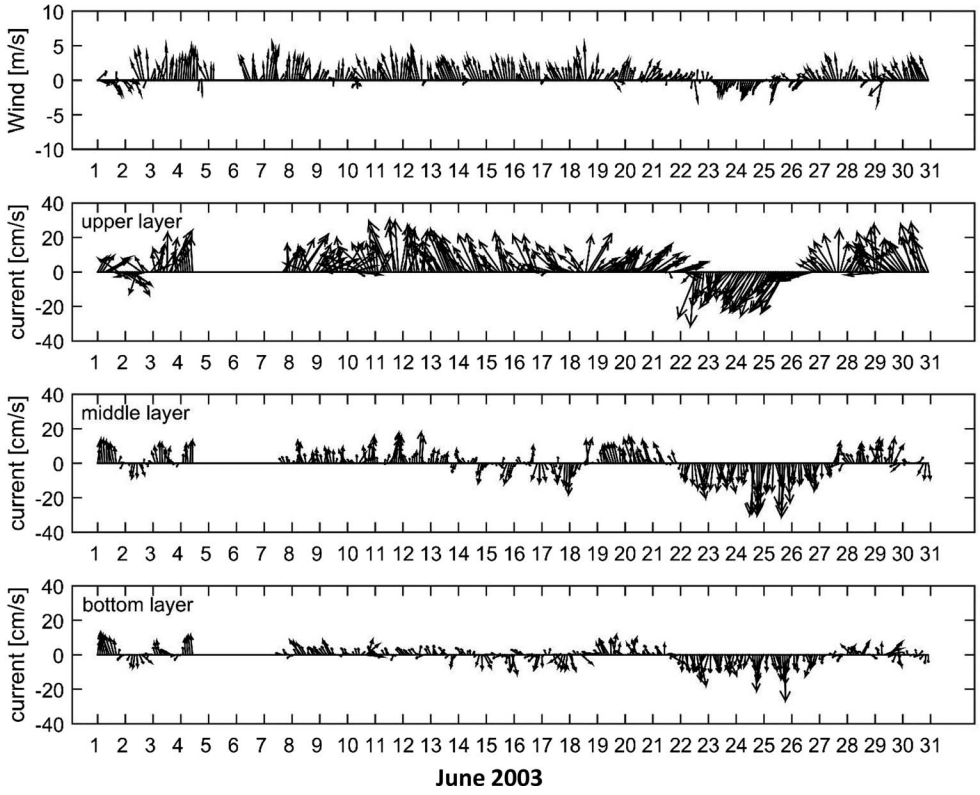

Figure 12. Time series of wind vectors (upper panel) and currents (three lower panels) at three elevations in the depth-normalized water column (0.95, 0.65, 0.35) during June 2003.

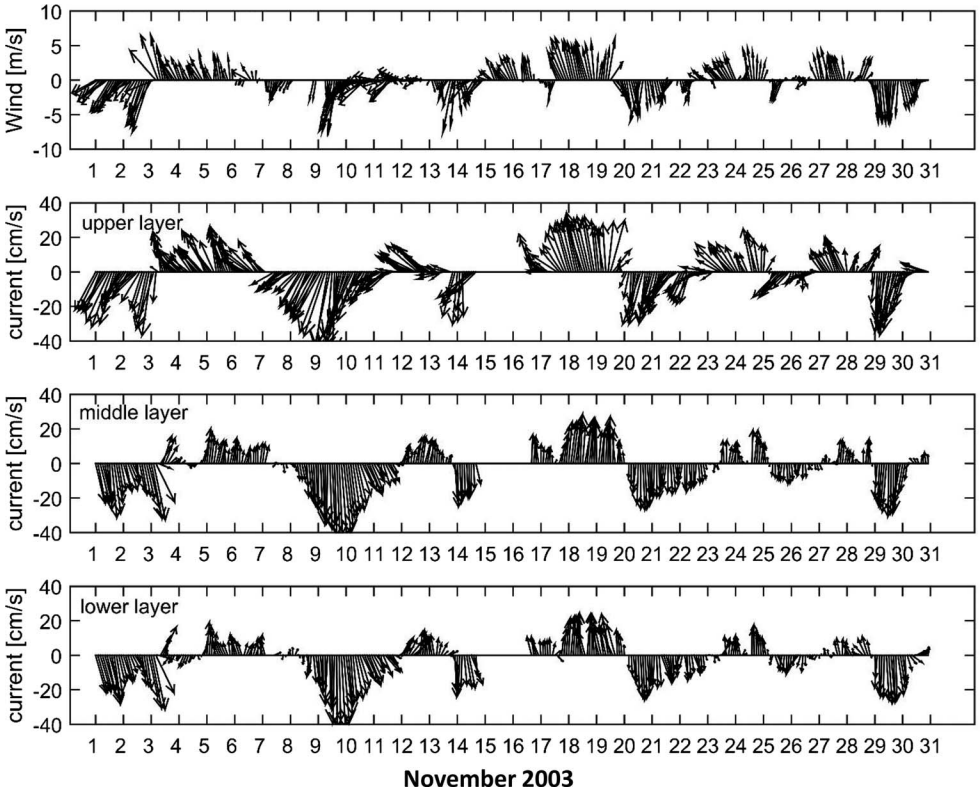

Figure 13. Time series of wind vectors (upper panel) and currents (three lower panels) at three elevations in the depth-normalized water column (0.95, 0.65, 0.35) during November 2003.

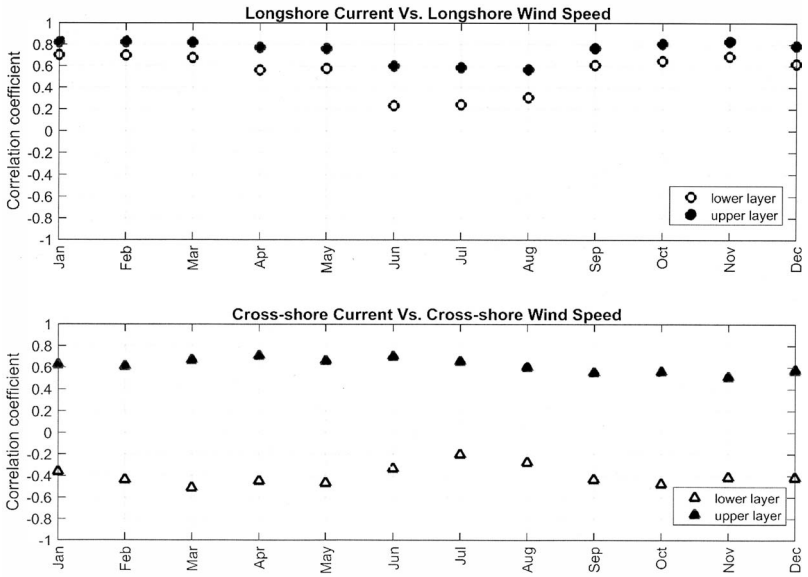

Figure 14. Composite year of monthly correlations between 2-hour-average time series of currents and 2-hour-average time series of longshore and cross-shore wind components at the upper (0.95) and lower (0.35) layers of the water column.

Table 2. *Average longshore and cross-shore wind stress.*

Year	Average Wind Stress (N/m^2)	
	Longshore (+ northerly)	Cross-Shore (+ offshore)
2002	−0.0008	−0.0101
2003	−0.0018	−0.0100
2004	0.0009	−0.0144
2005	−0.0007	−0.0150
2006	0.0016	−0.0008
2007	−0.0019	−0.0053
2008	0.0012	−0.0006
2009	0.0011	0.0009
2010	−0.0022	0.0014
2011	−0.0002	−0.0021
Mean	*−0.0003*	*−0.0056*
Stand. Dev.	*0.00135*	*0.00598*

In contrast, 2002, 2003, and 2010 were less active, with 4, 7, and 6 storms, respectively. The percentages of time during a storm that waves approached from the northeast ($\theta_{mean} < 69°$), shore-normal ($69° < \theta_{mean} < 77°$), and southeast ($\theta_{mean} > 77°$) directions were then computed for each year. For all the years, the percent of waves approaching shore-normal ($69° < \theta_{mean} < 77°$) during storms was similar, with an average of 27% and a standard deviation of 6%. For 2003, 2006, and 2009, the percent of waves approaching from the northeast was less than the percent of waves approaching from the southeast. For the remainder of the years, the percent of storm waves approaching from the northeast was significantly greater (39% to 61%) than the percent of storm waves approaching from the southeast (11% to 34%). Finally, based solely on storm forcing for the entire record, waves approached more frequently from the northeast during storms (40%) than from the southeast (33%), consistent with the expectation of net N-S transport in the long term.

The annual storm analysis prompted the computation of the correlations between the northerly and southerly directed longshore currents and the radiation stress in the longshore direction (S_{xy}), as is presented in Table 6. The computed correlations between the southerly longshore current speed

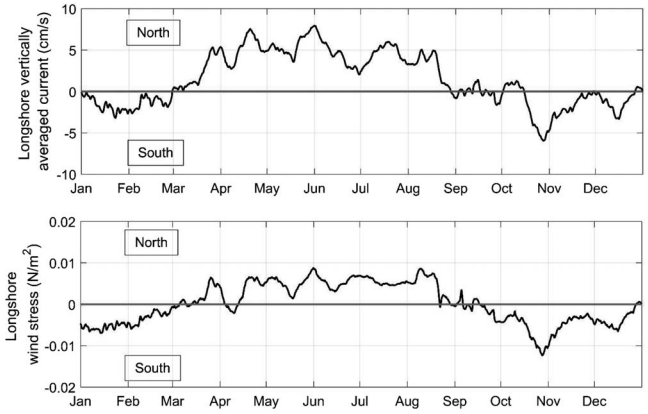

Figure 15. Composite year of the weekly running average of vertically averaged longshore current (upper panel) and composite year of the weekly running average of the longshore wind stress (lower panel).

Table 3. *Yearly averages of energy-based significant wave height (H_{mo}) at Spessard during northerly directed and southerly directed longshore currents for the 10 years of record.*

Year	Average H_{mo} (m) for Northerly Currents	Average H_{mo} (m) for Southerly Currents
2002	0.71	0.86
2003	0.67	0.90
2004	0.73	1.00
2005	0.73	1.06
2006	0.84	1.09
2007	0.83	0.97
2008	0.76	0.95
2009	0.70	0.91
2010	0.70	0.90
2011	0.67	0.86
Mean	*0.73*	*0.95*
Stand. Dev.	*0.056*	*0.076*

and the spectrally integrated radiation stress, Equation (1), was higher than the correlations between the northerly longshore current speed and the radiation stress for 2002, 2003, 2005, 2006, 2008, 2009, 2010, and 2011. For the combined 10 years, the average correlation between the southerly longshore current speed and S_{xy} (0.51) is higher than the average correlation between northerly currents and S_{xy} (0.33). Additionally, from Table 6, it is noted that for the storms with H_{mo} above 1.75 m, the percent of occurrences for the southerly directed longshore current is greater than the percent of occurrences for the northerly directed longshore current for every year except 2009. As a result, for the combined 10 years, the average percent of occurrence for the storm-associated southerly longshore current is 68%, which is significantly higher than the 32% for the northerly longshore current.

Winds and Currents During Landfalling Hurricanes

The top panel of Figure 16 presents wind measurements from the Trident station anemometer for September of 2004, during which Hurricanes Frances and Jeanne both made landfall in Stuart, Florida, nominally 130 km to the south of Port Canaveral. Although the Spessard ADCP missed the landfall of Frances on 5 September due to a premature power outage, the instrument was equipped after the storm with a bank of batteries in time to capture the landfall of Hurricane Jeanne on the 26 September. From the wind record, the similarity in

Table 4. *Yearly correlations between northerly and southerly depth-averaged longshore currents and* $H_{mo}^{5/2}$.

Year	Correlation of $H_{mo}^{5/2}$ with Northerly Longshore Current	Correlation of $H_{mo}^{5/2}$ with Southerly Longshore Current
2002	0.29	0.48
2003	0.18	0.42
2004	0.53	0.59
2005	0.08	0.55
2006	0.09	0.39
2007	0.18	0.63
2008	0.23	0.54
2009	0.31	0.28
2010	0.12	0.44
2011	0.08	0.40
Mean	*0.21*	*0.47*
Stand. Dev.	*0.134*	*0.101*

Table 5. *Annual storm count and percent occurrence of storm waves from the northeast, shore-normal, and southeast directions from the Spessard ADCP for the 10 years of record.*

		Percent Occurrence		
Year	Number of Storms ($H_{mo} > 1.75$ m)	Northeast $\theta_{mean} < 69°$	Shore-Normal $69° < \theta_{mean} < 77°$	Southeast $\theta_{mean} > 77°$
2002	4	39	27	34
2003	7	31	28	41
2004	11	44	22	34
2005	11	39	27	34
2006	12	28	24	48
2007	8	41	31	28
2008	11	61	28	11
2009	9	30	16	54
2010	6	47	29	24
2011[†]	11	36	40	24
Mean	*9*	*40*	*27*	*33*
Stand. Dev.	*2.5*	*9.2*	*5.9*	*11.8*

[†]*Wave record from 28 October to 31 December 2011 synthesized from hindcast modeling.*

magnitude and direction of the two hurricane events can be appreciated, where strong winds started blowing from N-S with a sudden change in direction of almost 180° at landfall. During Hurricane Jeanne, similar behavior is observed in the current measurements presented in the lower three panels of Figure 16, showing them to be nearly uniform with depth in the longshore direction, but with offshore return flow in the middle and lower layers. The maximum 10-minute current speeds, both northerly (1.2 m/s) and southerly (0.98 m/s), during Hurricane Jeanne were twice that of all other storms in the record. With the penetration of strong longshore currents all the way to the lower layer of the water column, one would expect significant longshore transport of sediment even far outside the surf zone during the landfall of the storm. The lower panel of Figure 16 suggests that the net transport over the entire storm was likely N-S, as there was a persistent and moderately strong southerly current from 19 to 25 September generated as Jeanne made a loop offshore before making landfall.

CONCLUSIONS

The methodology for extracting the tidal signal from the water surface by utilizing the data from the Trident Pier station worked effectively, enabling the water column to be normalized and measurements contaminated by surface echo to be eliminated. Decomposing each current measurement into longshore and cross-shore components produced time series that meaningfully represent the behavior of the vertical structure of the currents in the upper 70% of the water column for each one of the nearly 10 years of available data. In the future, incorporating a down-looking instrument installed above the blanking elevation of the ADCP would enable the entire water column to be examined. More importantly, however, long-term measurement of currents *inside* the surf zone would be more appropriate for answering some of the longshore transport questions raised herein. However, meaningful *in situ* measurements would probably require some sort of a self-positioning apparatus that could deal with the ever-changing tide and surf conditions in order to remain in the active surf zone, a technology that has not yet been developed.

It is clearly evident that yearly averages of the mean vertical profile do not substantially represent the true vertical structure of the currents at any particular time. This is mainly due to the large variability in both the wind and wave climate, which forces the nearshore current to change structure frequently. Consequently, the resulting mean current profile for a year has a small mean structure but with large standard deviation at every level of the normalized water column (Table A1). Computing basic statistics is useful in understanding the seasonal behavior of the vertical structure of the currents, with monthly averaged mean profiles revealing the tendency of the longshore current to flow toward the north during summer months and to flow toward the south during winter months. For most of the years, the mean profile of the longshore current is northerly directed in the upper layers of the water column and slightly southerly directed at the blanking elevation. The reason for this apparent reversal is unknown, but possible explanations include (1) residual astronomic tide-driven currents, (2) longshore return flow induced by the presence of Cape Canaveral and its large shoal complex located to the north, (3) flow induced by a large-scale indentation in the shelf bathymetry that exists offshore of Melbourne Beach, and/or (4) large-scale circulation induced by the Gulf Stream. Again, the residual mean longshore current profiles (Figure 7) have much smaller magnitudes than the variations about the mean (Appendix A), rendering an explanation problematic. For all the years, the mean profile of the cross-shore current shows significantly larger magnitudes in the upper layers of the water

Table 6. *Correlations and percent occurrence between the northerly and southerly directed longshore current and the radiation stress (S_{xy}) during storm events ($H_{mo} > 1.75$ m).*

Year	Correlation of Northerly Current and S_{xy}	Correlation of Southerly Current and S_{xy}	Northerly Current Occurrence (%)	Southerly Current Occurrence (%)
2002	0.53	0.79	29	71
2003	0.16	0.49	14	86
2004	0.90	0.01	23	77
2005	0.44	0.72	21	79
2006	0.03	0.69	38	62
2007	0.52	0.37	28	72
2008	0.32	0.44	45	55
2009	0.07	0.39	57	43
2010	−0.07	0.75	27	73
2011	0.40	0.46	41	59
Mean	*0.33*	*0.51*	*32*	*68*
Stand. Dev.	*0.277*	*0.225*	*12.2*	*12.2*

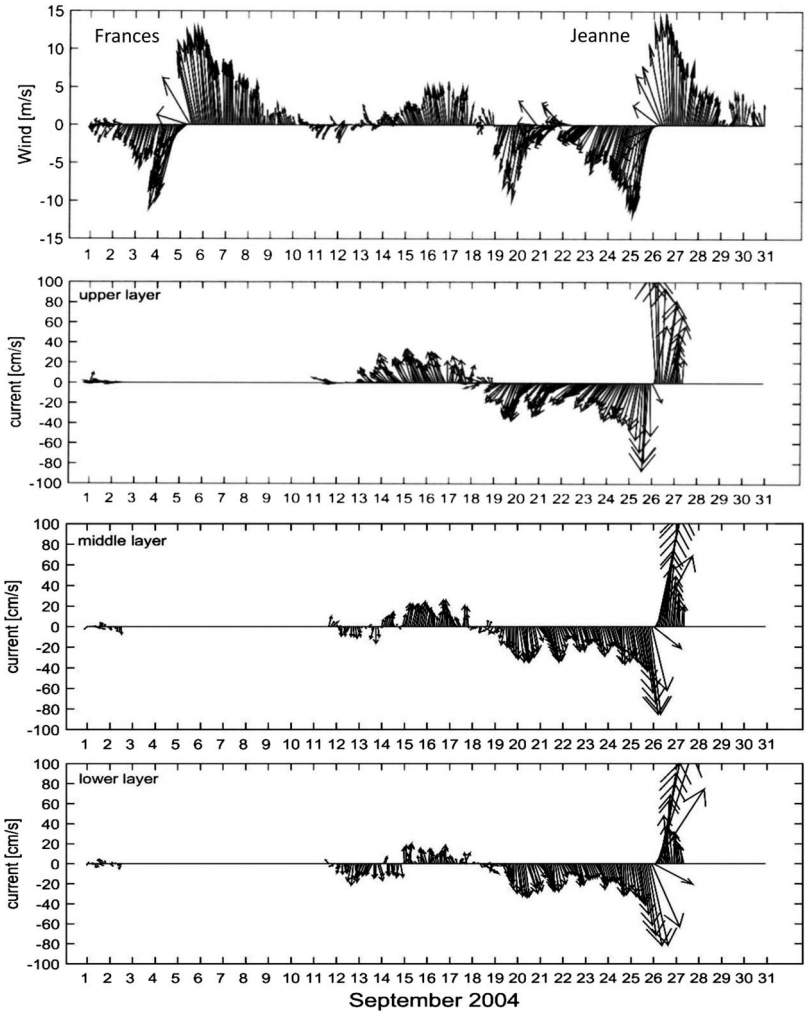

Figure 16. Time series of wind vectors (upper panel) during September 2004 showing Hurricane Frances (5 September 2004) and Hurricane Jeanne (26 September 2004), and currents (lower three panels) at three elevations in the depth-normalized water column (0.95, 0.65, 0.35) during Jeanne.

column than at the bottom, with one zero-crossing point, around 0.90 normalized elevation.

Monthly correlations between 2-hour block-averaged time series of longshore current and wind speed revealed some of the seasonal patterns of the wind and longshore current, in which the upper layer of the water column is highly correlated with the longshore component of the wind speed for most of the winter months, and it is less correlated for most of the summer months. The lower layer of the water column is less correlated with the wind, but it has similar patterns during winter and summer months. The cross-shore current at the upper layer of the water column is highly correlated with the cross-shore component of the wind speed for most of the winter months, and it is less correlated during the summer months. The negative correlation between the cross-shore current in the lower layer of the water column and the wind is due to the return flow required because of the nearby shoreline.

It appears that the enigma encountered by Montoya and Dally (2016), where (1) the long-term net radiation stress (S_{xy}) was only weakly N-S, and (2) the long-term net longshore wind stress was nearly balanced, whereas the shoreline offsets at nearby inlets would indicate a much stronger N-S bias, can be explained by a significantly higher correlation between southerly directed currents and incident wave energy flux than northerly directed currents and wave energy flux. This is also confirmed by the stronger correlation of southerly directed currents with both wave height and radiation stress during storm events ($H_{mo} > 1.75$ m). It is unknown if this enigma is as pronounced or even is found at other locations. The needed measurements do not exist, but preliminary examination of nearshore synthetic wave records from other locations on Florida's Atlantic coast (*e.g.*, Surfbreak Engineering Sciences Staff, 2009) indicates that this is the case. In any event, it is suggested that future research should attempt to incorporate this apparently important role of the wind and its correlation with wave forcing with the resulting currents and sand entrainment, either deterministically (*e.g.*, King, 2007) or stochastically. With more reliable longshore transport formu-

las, shoreline evolution modeling and coastal science and engineering as a whole will benefit.

ACKNOWLEDGMENTS

Past financial support for the collection of the wave data utilized herein was provided by the Florida Department of Environmental Protection (former) Bureau of Beaches and Coastal Systems, and the Program for the Study of Developed Shorelines, Western Carolina University, and it is gratefully acknowledged. The authors are indebted to Daniel A. Osiecki, who operated the data collection system from 2001 to 2009 while employed with Surfbreak Engineering Sciences, Inc. C.B. was financially supported by the Taylor Engineering Research Institute at the University of North Florida.

LITERATURE CITED

Bacopoulos, P.; Dally, W.R.; Hagen, S.C., and Cox, A.T., 2012. Observations and simulation of winds, surge, and currents on Florida's east coast during Hurricane Jeanne (2004). *Coastal Engineering*, 60, 84–94.

Battjes, J.A., 1972. Radiation stresses in short-crested waves. *Journal of Marine Research*, 30, 56–64.

Book, J.W.; Perkins, H.; Signell, R.P., and Wimbush, M., 2007. *The Adriatic Circulation Experiment Winter 2002/2003 Mooring Data Report: A Case Study in ADCP Data Processing*. Washington, D.C.: Naval Research Laboratory, *Report NRL/MR/7330-07-8999*, 50p.

Cosoli, S.; Gacic, M., and Mazzoldi, A., 2008. Variability of currents in front of the Venice Lagoon, northern Adriatic Sea. *Annales Geophysicae*, 26, 731–746.

Dally, W.R. and Osiecki, D.A., 2006. Development & validation of hindcast-driven nearshore wave information. *Proceedings of the 9th International Workshop on Wave Hindcasting and Forecasting* (Victoria, British Columbia, Canada). http://www.waveworkshop.org/9thWaves/.

Garrett, J.R., 1977. Review of drag coefficients over oceans and continents. *Monthly Weather Review*, 105(7), 915–929.

Gravens, M.B.; Kraus, N.C., and Hanson, H., 1991. *GENESIS: Generalized Model for Simulating Shoreline Change, Report 2, Workbook and System User's Manual*. Vicksburg, Mississippi: U.S. Army Engineer Waterways Experiment Station, Coastal Engineering Research Center, *Technical Report CERC-89-19*, 345p. plus appendices.

Hanson, H. and Kraus, N.C., 1989. *GENESIS: Generalized Model for Simulating Shoreline Change, Report 1, Technical Reference*. Vicksburg, Mississippi: U.S. Army Engineer Waterways Experiment Station, Coastal Engineering Research Center, *Technical Report CERC-89-19,* 185p. plus appendices.

Houghton, D. and Woods, J., 1969. The slippery seas of Acapulco. *New Scientist*, 16, 134–136.

Hubertz, J.M., 1986. Observations of local wind effects on longshore currents. *Coastal Engineering*, 10, 275–288.

King, D.B., 2007. *Wave and Beach Processes Modeling for Sabine Pass to Galveston Bay, Texas, Shoreline Erosion Feasibility Study*. Vicksburg, Mississippi: USACE Engineer Research and Development Center, *Technical Report ERDC/CHL TR-07-6*, 150p.

Komar, P.D., 1979. Beach-slope dependence of longshore currents. *Journal of Waterway, Port, Coastal, and Ocean Division, American Society of Civil Engineers*, 105(WW4), 460–464.

Longuet-Higgins, M.S., 1970. Longshore currents generated by obliquely incident sea waves, 2. *Journal of Geophysical Research,* 75(33), 6790–6801.

Luettich, R.A., Jr., and Westerink, J.J., 2004. *Formulation and Numerical Implementation of the 2D/3D ADCIRC Finite Element Model Version 44.XX*. http://www.unc.edu/ims/adcirc/publications/2004/2004_Luettich.pdf.

Montoya, L.H., 2014. Analysis of a 10-Year Nearshore Wave Database and its Implications to Littoral Processes. Jacksonville, Florida: University of North Florida, Master's thesis, 94p.

Montoya, L.H. and Dally, W.R., 2016. Analysis of a 10-year record of nearshore directional wave spectra and implications to littoral processes research and engineering practice. *Journal of Coastal Research*, 32(5), 1162–1173.

Münchow, A. and Chant, R.J., 2000. Kinematics of inner shelf motion during the summer stratified season off New Jersey. *Journal of Physical Oceanography*, 30(2), 247–268.

Murray, S.P., 1975. Trajectories and speeds of wind-driven currents near the coast. *Journal of Physical Oceanography,* 5(2), 347–360.

Nummedal, D. and Finley, R.J., 1978. Wind-generated longshore currents. *Proceedings of the 16th Coastal Engineering Conference* (Hamburg, Germany, ASCE), pp. 1428–1438.

Starr, V.P., 1947. Momentum and energy integrals for gravity waves of finite height. *Journal of Marine Research*, 6, 175–193.

Surfbreak Engineering Sciences Staff, 2009. *Development of a Nearshore Synthetic Wave Record for St. Johns County, Florida*. Winter Park, Florida: Surfbreak Engineering Sciences, Inc., 16p.

Svendsen, I.A. and Putrevu, U., 1994. Nearshore mixing and dispersion. *Proceedings of the Royal Society of London*, 445(1925), 561–576.

USACE (U.S. Army Corps of Engineers), 2002. *Coastal Engineering Manual*. Vicksburg, Mississippi: U.S. Army Engineering Research and Development Center, 111p.

Whitney, M.M. and Garvine, R.W., 2005. Wind influence on a coastal buoyant outflow. *Journal of Geophysical Research*, 110(C3), C030104. doi:10.1029/2003JC002261

APPENDIX A

Table A1. *Annually based statistics (mean, standard deviation, and maxima) for the longshore and cross-shore currents at five normalized elevations above the bottom. The standard deviation is generally an order of magnitude greater than the mean, and it diminishes monotonically with depth for the longshore current.*

		Longshore Current				Cross-Shore Current			
Year	Normalized Elevation above the Bottom	Mean (cm/s)	Standard Deviation (cm/s)	Max North (cm/s)	Max South (cm/s)	Mean (cm/s)	Standard Deviation (cm/s)	Max East (cm/s)	Max West (cm/s)
2002	0.95	3.6	15.6	55.4	−71.0	−4.8	6.2	49.5	−34.1
	0.8	3.0	13.5	64.1	−49.0	0.8	2.4	33.2	−35.9
	0.65	2.3	12.8	48.9	−47.6	0.5	1.8	29.9	−23.6
	0.5	1.3	11.8	48.1	−45.7	0.3	1.8	28.4	−20.2
	0.35	0.3	10.7	47.0	−46.4	0.3	2.0	30.8	−15.9
2003	0.95	1.1	15.5	47.0	−55.0	−3.6	5.7	23.8	−52.8
	0.8	−0.1	13.7	46.0	−50.6	1.0	2.4	33.6	−49.9
	0.65	−1.1	12.6	46.7	−48.9	0.5	2.0	33.3	−36.5
	0.5	−1.9	11.4	39.6	−49.1	0.1	1.9	27.3	−15.7
	0.35	−2.5	10.2	33.3	−49.0	0.1	2.1	17.2	−17.9
2004	0.95	4.3	16.9	*124.7*	*−97.8*	−3.7	5.6	22.2	−23.2
	0.8	3.4	14.9	117.1	−93.6	1.0	2.4	28.2	−17.9
	0.65	2.3	14.1	117.8	−95.4	0.6	2.1	28.4	−16.9
	0.5	0.9	13.1	119.8	−95.3	0.3	2.1	31.8	−10.2
	0.35	−0.3	12.0	118.7	−94.8	0.3	2.2	36.1	−8.9
2005	0.95	2.5	17.1	54.7	−54.0	−2.7	5.8	23.9	−27.6
	0.8	2.5	15.4	47.3	−47.0	0.9	2.5	24.2	−15.7
	0.65	1.6	14.5	43.5	−47.8	0.5	2.1	19.3	−21.8
	0.5	0.4	13.3	43.9	−48.9	0.2	2.1	17.4	−27.9
	0.35	−0.8	12.0	41.9	−47.0	0.1	2.3	15.2	−18.4
2006	0.95	6.0	16.1	48.3	−74.0	−3.7	5.8	22.6	−27.7
	0.8	4.5	14.4	52.1	−68.4	1.0	2.7	19.8	−15.9
	0.65	3.2	13.3	51.1	−65.8	0.5	2.1	18.6	−15.0
	0.5	1.5	12.0	47.3	−65.0	0.2	2.0	20.7	−10.6
	0.35	0.0	10.5	34.1	−63.9	0.2	2.3	16.3	−13.8
2007	0.95	1.6	16.9	49.6	−62.1	−3.7	6.8	28.4	−26.5
	0.8	1.0	14.4	48.0	−54.7	1.1	2.7	22.3	−14.1
	0.65	0.2	13.4	46.9	−52.1	0.8	2.1	17.3	−10.6
	0.5	−0.8	12.1	46.1	−48.2	0.7	2.0	16.8	−13.3
	0.35	−1.7	10.8	44.0	−46.0	0.7	2.2	15.1	−11.8
2008	0.95	3.0	17.5	63.1	−67.7	−4.6	6.4	30.6	−38.2
	0.8	3.3	15.9	66.8	−58.1	0.7	4.4	96.5	*−103.9*
	0.65	2.3	14.8	54.0	−55.9	0.3	3.2	81.2	−92.7
	0.5	1.1	13.3	47.4	−55.1	0.2	2.4	25.7	−23.7
	0.35	−0.3	11.4	36.9	−55.5	0.4	2.7	17.5	−12.9
2009	0.95	3.9	14.8	70.9	−68.0	−2.3	6.7	77.4	−82.8
	0.8	3.5	14.2	77.9	−56.4	0.5	4.7	*130.9*	−61.1
	0.65	2.3	13.2	54.1	−49.6	0.0	3.5	72.0	−48.6
	0.5	1.0	12.2	35.5	−46.5	−0.1	3.0	20.4	−19.0
	0.35	−0.2	10.7	33.5	−44.9	0.0	3.1	17.3	−14.8
2010	0.95	2.8	16.0	56.7	−67.3	−2.0	6.8	31.8	−37.1
	0.8	2.3	13.5	48.9	−55.0	0.5	4.4	32.1	−23.6
	0.65	1.1	12.2	43.3	−53.0	0.2	3.6	29.4	−20.5
	0.5	−0.2	10.9	37.6	−49.2	0.2	3.2	27.1	−17.5
	0.35	−1.7	9.7	31.0	−46.6	0.4	3.3	25.9	−16.3
2011	0.95	5.0	14.8	53.1	−98.7	−2.5	8.4	56.6	−47.8
	0.8	4.4	12.7	66.9	−87.8	0.6	4.6	50.0	−43.0
	0.65	3.3	11.5	51.3	−83.1	0.2	3.7	51.7	−32.7
	0.5	1.9	10.4	35.7	−81.2	0.1	3.4	46.1	−25.5
	0.35	0.1	9.2	33.2	−77.6	0.3	3.6	41.0	−23.1